

Benchmarking Λ NN three-body forces and first predictions for $A = 3 - 5$ hypernuclei

Hoai Le^{1,a}, Johann Haidenbauer^{1,b}, Hiroyuki Kamada^{2,3,c,d}, Michio Kohno^{3,e}, Ulf-G. Meißner^{4,1,5,f}, Kazuya Miyagawa^{3,g}, Andreas Nogga^{1,5,h}

¹Institute for Advanced Simulation (IAS-4), Forschungszentrum Jülich, D-52425 Jülich, Germany

²Department of Physics, Faculty of Engineering, Kyushu Institute of Technology, Kitakyushu 804-8550, Japan

³Research Center for Nuclear Physics, Osaka University, Ibaraki 567-0047, Japan

⁴Helmholtz-Institut für Strahlen- und Kernphysik and Bethe Center for Theoretical Physics, Universität Bonn, D-53115 Bonn, Germany

⁵CASA, Forschungszentrum Jülich, D-52425 Jülich, Germany

March 1, 2024

Abstract Explicit expressions for the leading chiral hyperon-nucleon-nucleon three-body forces have been derived by Petschauer et al [Phys. Rev. C93.014001 (2016)]. An important prerequisite for including these three-body forces in few- and many-body calculations is the accuracy and efficiency of their partial-wave decomposition. A careful benchmark of the Λ NN potential matrix elements, computed using two robust and efficient partial-wave decomposition methods, is presented. In addition, results of a first quantitative assessment for the contributions of Λ NN forces to the separation energies in $A = 3 - 5$ hypernuclei are reported.

1 Introduction

Few-nucleon systems have served as a crucial testing ground for our understanding of nucleon-nucleon (NN) and three-nucleon (3N) forces [1–10]. In the course of this, due to the complexity of the computational treatment of few-body systems and the goal of achieving accurate predictions using realistic nuclear forces, it has become standard to cross-compare results achieved with various methods and by independent research groups. Indeed, such benchmark studies have become an integral part of the advancement of microscopic few-nucleon calculations. For instance, in the past, benchmark results have been produced for nucleon-deuteron (N-d)

scattering [11, 12], for N-d breakup [13], for the triton binding energy including 2π exchange three-nucleon forces [14], for the four-nucleon (4N) bound state [15] and for 4N scattering [16, 17].

Regarding strangeness nuclear physics realistic calculations of Λ hypernuclei including the full complexity of the Λ N- Σ N interaction were first presented in [18, 19] for the hypertriton and in [20–22] for ${}^4_{\Lambda}\text{H}$ and ${}^4_{\Lambda}\text{He}$. Both are momentum-space calculations based on the Faddeev- and Faddeev-Yakubovsky (FY) approaches, respectively. Very recently, the first calculations of the hypertriton separation energy including chiral Λ NN three-body forces (3BFs) [23] have been published [24, 25]. Actual benchmark studies for hypernuclei are however scarce. Over the years, a diverse range of calculations employing various methods [22, 26–34] have been carried out. However, the elementary NN and hyperon-nucleon (YN) potentials utilized as input in those calculations are very different, making a comprehensive comparison of the results not possible. On the other hand, an actual benchmark study for few-body hypernuclei presented in Ref. [35] relied on rather simple representations of the NN and YN interactions. Only lately, first elaborate benchmark results for ${}^4_{\Lambda}\text{H}$ [33] were reported, by comparing calculations based on the FY equations and the Jacobi no-core shell model (Jacobi-NCSM), for state-of-the-art NN and YN two-body interactions, namely the so-called SMS NN potentials derived within chiral effective field theory (EFT) [36] and YN interactions established likewise in chiral EFT [37, 38].

With the present work we want to add a further benchmark for Λ hypernuclei. Specifically, we provide a detailed comparison of the calculations by Kamada, Kohno, and Miyagawa (KKM) [24, 25] and the Jülich-Bonn Group (JBG) [39, 40] for the hypertriton includ-

^ae-mail: h.le@fz-juelich.de

^be-mail: j.haidenbauer@fz-juelich.de

^ce-mail: kamada@mns.kyutech.ac.jp

^de-mail: kamada@rcnp.osaka-u.ac.jp

^ee-mail: kohno@rcnp.osaka-u.ac.jp

^fe-mail: meissner@hiskp.uni-bonn.de

^ge-mail: miyagawa@rcnp.osaka-u.ac.jp

^he-mail: a.nogga@fz-juelich.de

ing chiral 3BFs. The former calculation is performed within the Faddeev approach while the latter utilizes the Jacobi-NCSM formalism. The motivation for our study originates from discrepancies in the contribution of the 2π exchange Λ NN force to the hypertriton separation energy observed between the KKM results [24] and the preparatory calculations of JBG. In the course of clarifying them [41], it became clear that it would be rather useful to provide an in-depth comparison of the results by the two groups, which does not only shed light on the accuracy of the two methods but also allows for an examination of the underlying technical and numerical aspects of such complex calculations. Clearly, such a detailed comparison is not only indispensable for corroborating the outcome of the present three-body calculations, but it provides also a useful guideline for future calculations employing different few-body methods.

The paper is organized as follow. In the following section, we briefly describe the two approaches for the partial-wave decomposition of the Λ NN (and Σ NN) potentials employed by KKM and JBG. A detailed comparison of the Λ NN potential matrix elements in different partial-wave states are presented in Sect. 3. In Sect. 4 we discuss possible contributions of the chiral Λ NN interaction to the separation energies in the $A = 3 - 5$ hypernuclei and we close with some concluding remarks.

2 Partial-wave decomposition of the chiral YNN forces

The generic contact, one- and two-meson exchange diagrams for the process $B_1 B_2 B_3 \rightarrow B_4 B_5 B_6$, appearing at next-to-next-to-leading order (N^2 LO) in the chiral expansion [23], are shown in panels (a), (b) and (c) in Fig. 1, respectively. The fully antisymmetrized contact YNN potential, obtained from the diagram (a) in Fig. 1 and all the permutations of the incoming $B_1 B_2 B_3$ and outgoing $B_4 B_5 B_6$ baryon states, is given by [23, 42]

$$V_{\text{ct}} = - \left[N_{123}^{1456} + N_{123}^{2456} \vec{\sigma}_A \cdot \vec{\sigma}_B + N_{123}^{3456} \vec{\sigma}_A \cdot \vec{\sigma}_C + N_{123}^{4456} \vec{\sigma}_B \cdot \vec{\sigma}_C + N_{123}^5 i \vec{\sigma}_A \cdot (\vec{\sigma}_B \times \vec{\sigma}_C) \right], \quad (1)$$

where N_{123}^i are appropriately antisymmetrized combinations of the 18 LECs defined in Eq. (18) of Ref. [23]. The one-meson exchange potential corresponding to the master diagram (b) in Fig. 1 reads,

$$V_{1\text{me}} = \frac{1}{2f_0^2} \frac{\vec{\sigma}_A \cdot \vec{q}_i}{\vec{q}_i^2 + m_\phi^2} \left[N_1 \vec{\sigma}_C \cdot \vec{q}_i + N_2 i (\vec{\sigma}_B \times \vec{\sigma}_C) \vec{q}_i \right], \quad (2)$$

with $\vec{q}_i = \vec{p}_i - \vec{p}'_i$ the transferred momentum. Explicit expressions for the constants N_1, N_2 are given by Eq. (30) in Ref. [23]. Based on the general expression in Eq. (2), the antisymmetrized one-meson exchange $B_1 B_2 B_3 \rightarrow B_4 B_5 B_6$ potential can be obtained by summing up for each exchange meson ϕ the 36 permutations of the initial and final baryons. Finally, the two-meson exchange diagram (c) yields

$$V_{2\text{me}} = - \frac{1}{4f_0^4} \frac{\vec{\sigma}_A \cdot \vec{q}_i \vec{\sigma}_C \cdot \vec{q}_{nk}}{(\vec{q}_i^2 + m_{\phi_1}^2)(\vec{q}_{nk}^2 + m_{\phi_2}^2)} \times [N'_1 + N'_2 \vec{q}_i \cdot \vec{q}_{nk} + N'_3 i (\vec{q}_i \times \vec{q}_{nk}) \cdot \vec{\sigma}_B]. \quad (3)$$

The constants $N'_{1,2,3}$ are defined in Eq. (34) in Ref. [23]. Similarly, summing up Eq. (3) for all the 18 permutations¹ of the initial and final baryon states and all possible exchanged mesons, one obtains the general antisymmetrized two-meson exchange YNN potential. Note that, in the calculations by JBG, all the coefficients N_{123}^i, N_i and N'_i in Eqs. (1-3) have been evaluated as functions of the involving LECs using *Mathematica*.

For the case of Λ NN \rightarrow Λ NN 3BFs that involve only π -meson exchanges, the expressions for the V^{Λ NN potentials in Eqs. (1-3) can be simplified significantly [23],

$$V_{\text{ct}}^{\Lambda$$
NN} = C'_1 (1 - \vec{\sigma}_2 \cdot \vec{\sigma}_3)(3 + \vec{\tau}_2 \cdot \vec{\tau}_3) + C'_2 \vec{\sigma}_1 \cdot (\vec{\sigma}_2 + \vec{\sigma}_3)(1 - \vec{\tau}_2 \cdot \vec{\tau}_3) + C'_3 (3 + \vec{\sigma}_2 \cdot \vec{\sigma}_3)(1 - \vec{\tau}_2 \cdot \vec{\tau}_3), \quad (4)

$$V_{1\pi}^{\Lambda$$
NN} = - \frac{g_A}{2f_0^2} \left(\frac{\vec{\sigma}_2 \cdot \vec{q}_{52}}{\vec{q}_{52}^2 + m_\pi^2} \vec{\tau}_2 \cdot \vec{\tau}_3 \left[(D'_1 \vec{\sigma}_1 + D'_2 \vec{\sigma}_3) \cdot \vec{q}_{52} \right] + \frac{\vec{\sigma}_3 \cdot \vec{q}_{63}}{\vec{q}_{63}^2 + m_\pi^2} \vec{\tau}_2 \cdot \vec{\tau}_3 \left[(D'_1 \vec{\sigma}_1 + D'_2 \vec{\sigma}_2) \cdot \vec{q}_{63} \right] + P_{23}^{(\sigma)} P_{23}^{(\tau)} P_{13}^{(\sigma)} \frac{\vec{\sigma}_2 \cdot \vec{q}_{62}}{\vec{q}_{62}^2 + m_\pi^2} \vec{\tau}_2 \cdot \vec{\tau}_3 \times \left[- \frac{D'_1 + D'_2}{2} (\vec{\sigma}_1 + \vec{\sigma}_3) \cdot \vec{q}_{62} + \frac{D'_1 - D'_2}{2} i (\vec{\sigma}_3 \times \vec{\sigma}_1) \cdot \vec{q}_{62} \right] + P_{23}^{(\sigma)} P_{23}^{(\tau)} P_{12}^{(\sigma)} \frac{\vec{\sigma}_3 \cdot \vec{q}_{53}}{\vec{q}_{53}^2 + m_\pi^2} \vec{\tau}_2 \cdot \vec{\tau}_3 \times \left[- \frac{D'_1 + D'_2}{2} (\vec{\sigma}_1 + \vec{\sigma}_2) \cdot \vec{q}_{53} - \frac{D'_1 - D'_2}{2} i (\vec{\sigma}_1 \times \vec{\sigma}_2) \cdot \vec{q}_{53} \right] \right), \quad (5)

¹The contribution from those permutations that yield identical results to the diagram in (c) is already included in Eq. (3), which explains for the factor of 18 instead of 36.

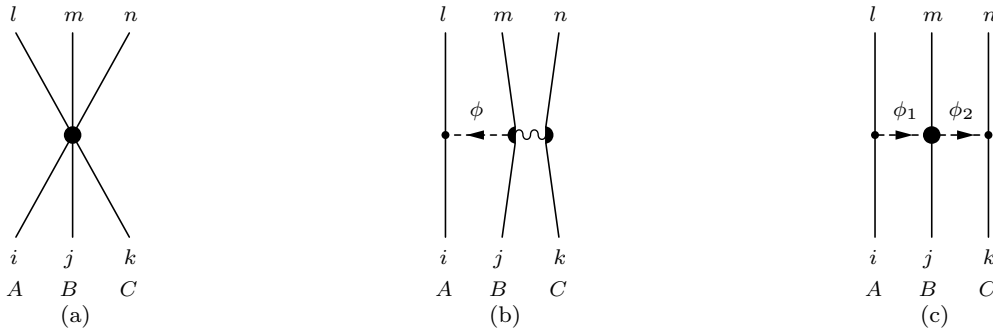


Fig. 1: Generic $YNN \rightarrow YNN$ diagrams: (a) contact term, (b) one-meson exchange, (c) two-meson exchange. The wiggly line symbolized the four-baryon contact vertex, to illustrate the baryon bilinears.

and,

$$\begin{aligned}
 V_{2\pi}^{\text{ANN}} = & \frac{g_A^2}{3f_0^4} \frac{\vec{\sigma}_3 \cdot \vec{q}_{63} \vec{\sigma}_2 \cdot \vec{q}_{52}}{(\vec{q}_{63}^2 + m_\pi^2)(\vec{q}_{52}^2 + m_\pi^2)} \vec{\tau}_2 \cdot \vec{\tau}_3 \\
 & \times \left(-(3b_0 + b_D)m_\pi^2 + (2b_2 + 3b_4) \vec{q}_{63} \cdot \vec{q}_{52} \right) \\
 - P_{23}^{(\sigma)} P_{23}^{(\tau)} & \frac{g_A^2}{3f_0^4} \frac{\vec{\sigma}_3 \cdot \vec{q}_{53} \vec{\sigma}_2 \cdot \vec{q}_{62}}{(\vec{q}_{53}^2 + m_\pi^2)(\vec{q}_{62}^2 + m_\pi^2)} \vec{\tau}_2 \cdot \vec{\tau}_3 \\
 & \times \left(-(3b_0 + b_D)m_\pi^2 + (2b_2 + 3b_4) \vec{q}_{53} \cdot \vec{q}_{62} \right). \quad (6)
 \end{aligned}$$

Here, the C'_i, D'_i, b_i are low-energy constants (LECs), the latter can in principle be fixed from the octet baryon masses and three-flavor meson-baryon scattering [43]. Note that, when the potentials in Eqs. (1-6) are applied to basis wave functions YNN (ANN) for which the two-nucleon states are antisymmetric, a scaling factor of $\frac{1}{2}$ [24, 25, 44] is required.

In order to include the above YNN (ANN) interactions in few- and many-body hypernuclear calculations, efficient and accurate methods for the partial-wave decomposition of these potentials are of importance. Therefore, in this study, we want to benchmark the chiral potential matrix elements V^{ANN} evaluated using two different partial-wave decomposition methods. In the first approach, referred to as IPWD, the locality of the chiral ANN potentials in Eqs. (4-6) is explicitly exploited so that the eight-fold integration over the angles of the incoming and outgoing momenta can be reduced to a two-fold integration, which in turn can significantly speed up the generation of the 3BF matrix elements. This method has initially been applied to the local chiral 3NFs up to $N^3\text{LO}$ by Hebeler et al [45], and recently extended by KKM [44] to compute the partial-wave decomposition matrix elements of the chiral ANN 3BF at $N^2\text{LO}$ based on Eqs. (4-6). In the method of KKM, the ANN interactions are rewritten in the tensor product form by separating the spin and angular-momentum parts and a convenient expression in a form similar to the Wigner-Eckart theorem is derived for the matrix element of the angle-dependent term. For more

details, one can refer to [44]. In the second approach, utilized by JBG and referred to as aPWD, the technique introduced by Skibinski et al. in Ref. [46] is employed to automatically perform the partial-wave decomposition of both ΛNN and ΣNN potentials using the general expressions in Eqs. (1-3).

In general, the three-body YNN partial-wave states $|p_{12}q_3\alpha_{\text{YNN}}\rangle$ with the total angular momentum J and total isospin T in jj -coupling can be constructed as follows

$$\begin{aligned}
 |p_{12}q_3\alpha_{\text{YNN}}\rangle & \\
 = |p_{12}q_3(l_{12}s_{12})j_{12}(l_3\frac{1}{2})J_3(j_{12}I_3)JM_J, (t_{12}t_Y)TM_T\rangle, & \quad (7)
 \end{aligned}$$

where p_{12} and q_3 are the relative Jacobi momenta between two nucleons and between the center-of-mass of two nucleons and the hyperon, respectively, and α_{YNN} denotes a set of discrete quantum numbers characterizing the state. In the first step of the aPWD, the 3BF YNN matrix elements are calculated in the partial-wave state in LS -coupling, $|p_{12}q_3\beta_{\text{YNN}}\rangle$,

$$\begin{aligned}
 |p_{12}q_3\beta_{\text{YNN}}\rangle & \\
 = |p_{12}q_3(l_{12}l_3)L(s_{12}\frac{1}{2})S(L, S)JM_J, (t_{12}t_Y)TM_T\rangle. & \quad (8)
 \end{aligned}$$

The LS -coupling representation $|p_{12}q_3\beta_{\text{YNN}}\rangle$ is related to the basis $|p_{12}q_3\alpha_{\text{YNN}}\rangle$ in Eq. (7) simply via a $9j$ symbol and Clebsch-Gordan coefficients [47]. In the basis $|p_{12}q_3\beta_{\text{YNN}}\rangle$, the 3BF YNN matrix elements can be

expressed as

$$\begin{aligned}
& \langle p'_{12}q'_3\beta'_{\text{YNN}}|V_{\text{YNN}}|p_{12}q_3\beta_{\text{YNN}}\rangle = \\
& \int d\hat{p}'_{12} \int d\hat{q}'_3 \int d\hat{p}_{12} \int d\hat{q}_3 \\
& \sum_{m_{L'}} C(L'S'J'; m_{L'}, M_{J'} - m_{L'}, M_{J'}) \mathcal{Y}_{l'_{12}l'_3}^{*L', m_{L'}}(\hat{p}'_{12}\hat{q}'_3) \\
& \sum_{m_L} C(LSJ; m_L, M_J - m_L, M_J) \mathcal{Y}_{l_{12}l_3}^{L, m_L}(\hat{p}_{12}\hat{q}_3) \\
& \langle p'_{12}q'_3 (s'_{12}\frac{1}{2}) S' M_{J'} - m_{L'}(t'_{12}, t_{Y'}) T' M_T | V^{\text{YNN}} | \\
& p_{12}q_3 (s_{12}\frac{1}{2}) S M_J - m_L(t_{12}, t_Y) T M_T \rangle,
\end{aligned} \tag{9}$$

where

$$\begin{aligned}
\mathcal{Y}_{l_{12}l_3}^{L, m_L}(\hat{p}_{12}\hat{q}_3) &= \sum_{m_{l_{12}}=-l_{12}}^{l_{12}} C(l_{12}, l_3, L; m_{l_{12}}, m_L - m_{l_{12}}, m_L) \\
&\times Y_{l_{12}, m_{l_{12}}}(\hat{p}_{12}) Y_{l_3, m_L - m_{l_{12}}}(\hat{q}_3).
\end{aligned} \tag{10}$$

The matrix elements in the spin- and isospin-spaces in Eq. (9), $\langle p'_{12}q'_3 (s'_{12}\frac{1}{2}) S' M_{J'}(t'_{12}, t_{Y'}) T' M_T | V^{\text{YNN}} | p_{12}q_3 (s_{12}\frac{1}{2}) S M_J(t_{12}, t_Y) T M_T \rangle$, depend on the momenta, spin- and isospin-quantum numbers of the incoming and outgoing states. They can be computed in analytic form as a function of the momenta p_{12}, q_3 and p'_{12}, q'_3 for all combinations of spin and isospin-quantum numbers utilizing a software for symbolic calculations such as *Maple* (in our case) or *Mathematica* [46]. This symbolic software also allows an automatic generation of a FORTRAN code for these matrix elements, so that the multifold integration over the angular part in Eq. (9) can efficiently be calculated numerically using a FORTRAN program. Furthermore, given that the 3BFs V^{YNN} is rotationally invariant, the matrix elements in Eq. (9) vanish unless $J = J'$ and $M_J = M_{J'}$, and in addition, they do not depend on the magnetic quantum number M_J , hence

$$\begin{aligned}
& \langle p'_{12}q'_3\beta'_{\text{YNN}}|V_{\text{YNN}}|p_{12}q_3\beta_{\text{YNN}}\rangle = \\
& \int d\hat{p}'_{12} \int d\hat{q}'_3 \int d\hat{p}_{12} \int d\hat{q}_3 \frac{1}{2J+1} \sum_{m_J=-J}^J \\
& \sum_{m_{L'}} C(L'S'J'; m_{L'}, M_J - m_{L'}, M_J) \mathcal{Y}_{l'_{12}l'_3}^{*L', m_{L'}}(\hat{p}'_{12}\hat{q}'_3) \\
& \sum_{m_L} C(LSJ; m_L, M_J - m_L, M_J) \mathcal{Y}_{l_{12}l_3}^{L, m_L}(\hat{p}_{12}\hat{q}_3) \\
& \langle p'_{12}q'_3 (s'_{12}\frac{1}{2}) S' M_J - m_{L'}(t'_{12}, t_{Y'}) T' M_T | V^{\text{YNN}} | \\
& p_{12}q_3 (s_{12}\frac{1}{2}) S M_J - m_L(t_{12}, t_Y) T M_T \rangle.
\end{aligned} \tag{11}$$

Since the integrand in Eq. (11) is a scalar, one can therefore freely chose the directions of the momenta, say p'_{12} and q'_3 such that $\vec{p}'_{12} = (0, 0, p_{12})$ and $\phi_{q_3} = 0$. As a consequence, the eight-fold integration in Eq. (11) can be effectively reduced to a five-fold integration [46],

$$\int d\hat{p}'_{12} \int d\hat{q}'_3 \int d\hat{p}_{12} \int d\hat{q}_3 \rightarrow \int d\theta_{q_3} \int d\hat{p}_{12} \int d\hat{q}_3,$$

which, in turn, can lead to a significant speed-up of the generation of the 3BF matrix-elements. Once the 3BF matrix elements in the LS -representation are known, the recoupling to the jj -basis, $\langle p'_{12}q'_3\alpha'_{\text{YNN}}|V_{\text{YNN}}|p_{12}q_3\alpha_{\text{YNN}}\rangle$, can easily be done [47]. In addition, since we assume that the 3BF YNN is charge independent, it is therefore sufficient to compute the matrix elements in Eq. (11) for a specific value of m_T , say $m_T = 0$.

3 Benchmarking ANN matrix elements

We are now in a position to benchmark the 3BF matrix elements computed using the two different partial-wave decomposition approaches described in the previous section. Since the IPWD method has only been implemented for the ANN potential, we will focus on comparing the ANN potential matrix elements and turn off the Σ components in the aPWD approach also for the binding energy calculations discussed later. In Table 1, we list the quantum numbers of the α_{ANN} states with positive parity and the total angular momentum and isospin of $(J^\pi, T) = (1/2^+, 0)$ and $(3/2^+, 0)$ which have been selected for benchmarking. The 2π -exchange ANN matrix elements, $\langle p'_{12}q'_3\alpha'_{\text{ANN}}|V_{2\pi}|p_{12}q_3\alpha_{\text{ANN}}\rangle$, computed at fixed Jacobi momenta

$p'_{12} = p_{12} = q_3 = 0.205507 \text{ fm}^{-1}$ and $q'_3 = 0.306967 \text{ fm}^{-1}$ are presented in Table 2. The sub-leading meson-baryon LECs [23], appearing in $V_{2\pi}^{\text{ANN}}$, have been set to $3b_0 + b_D = 0$ and $2b_2 + 3b_4 = -3.0 \times 10^{-3} \text{ MeV}^{-1}$. One can clearly observe almost perfect agreement between the aPWD and IPWD 2π -exchange ANN matrix elements.

Table 3 lists the 1π -exchange and contact ANN matrix elements in the partial-wave state with $(J^\pi, T) = (1/2^+, 0)$. The LECs in Eqs. (4, 5) are set to $D'_1 = 0$, $D'_2 = \frac{2C}{9f_0^2\Delta} = 0.6268 \text{ fm}^3$ with $C = 3/4 g_A = 0.9525$, $f_0 = 93 \text{ MeV}$, $\Delta = 300 \text{ MeV}$ and $C'_2 = 0$, $C'_1 = C'_3 = \frac{1}{72f_0^4\Delta} = 0.1852 \text{ fm}^5$ within the so-called decuplet saturation scheme. We do not show here the results in the $(J^\pi, T) = (3/2^+, 0)$ state but stress that similar agreement of better than 0.5% is also observed for the 1π -exchange and contact potential matrix elements in this partial-wave state. Fig. 2 shows the aPWD and IPWD 1π - and 2π -exchange ANN matrix elements, $\langle p'_{12}, q'_3, \alpha'_{\text{ANN}} | V^{\text{ANN}} | p_{12}, q_3, \alpha_{\text{ANN}} \rangle$ in the partial-wave

(J^π, T)	α_{ANN}	l_{12}	s_{12}	J_{12}	t_{12}	l_Λ	$2I_\Lambda$
$(1/2^+, 0)$	1	0	1	1	0	0	1
	2	2	1	1	0	0	1
	3	1	0	1	0	1	1
$(3/2^+, 0)$	1	0	1	1	0	0	1
	2	2	1	1	0	0	1
	3	1	0	1	0	1	1

Table 1: Quantum numbers of the first three ΛNN partial-wave states for the two selected J^π and T .

α'_{ANN}	α_{ANN}	J=1/2 ⁺ , T=0			J=3/2 ⁺ , T=0		
		aPWD	IPWD	diff [%]	aPWD	IPWD	diff [%]
1	1	0.211808E-03	0.211795E-03	0.01	0.211818E-03	0.211795E-03	0.01
2	1	0.488366E-03	0.488674E-03	0.06	0.488367E-03	0.488674E-03	0.06
3	1	0.200297E-03	0.200317E-03	0.01	-0.100145E-03	-0.100158E-03	0.01
1	2	0.488614E-03	0.488674E-03	0.01	0.488511E-03	0.488674E-03	0.03
2	2	-0.781242E-04	-0.781013E-04	0.03	-0.781352E-04	-0.781013E-04	0.04
3	2	0.504514E-04	0.504487E-04	0.01	-0.252244E-04	-0.252244E-04	
1	3	0.112725E-03	0.112723E-03	0.002	-0.563600E-04	-0.563617E-04	0.03
2	3	0.341903E-04	0.341810E-04	0.03	-0.170948E-04	-0.170905E-04	0.02
3	3	0.779062E-04	0.779012E-04	0.01	0.779025E-04	0.779012E-04	0.02

Table 2: 2π -exchange ΛNN matrix elements $\langle p'_{12}q'_3\alpha'_{\text{ANN}} | V_{2\pi} | p_{12}q_3\alpha_{\text{ANN}} \rangle$ in fm^5 , computed with the automatic partial-wave decomposition (aPWD) and the approach that exploits the locality of the chiral YNN interaction (IPWD). The incoming and outgoing momenta are fixed to $p'_{12} = p_{12} = q_3 = 0.205507 \text{ fm}^{-1}$ and $q'_3 = 0.306967 \text{ fm}^{-1}$. The sub-leading meson-baryon LECs [23] are set to $3b_0 + b_D = 0$ and $2b_2 + 3b_4 = -3.0 \times 10^{-3} \text{ MeV}^{-1}$.

state $(1/2^+, 0)$, as a function of the momentum p_{12} for $p'_{12} = q'_3 = q_3 = 0.20550664 \text{ fm}^{-1}$. Note that the matrix elements in Fig. 2 have been regularized employing a non-local regularization function of the form $f_\Lambda(p_{12}, q_3) = \exp(-(p_{12}^2 + \frac{3}{4}q_3^2)/\Lambda^4)$ with a cutoff of $\Lambda = 550 \text{ MeV}$. Such a non-local regularization function has the advantage that it does not depend on the angles and therefore can be applied to the potential independently of the partial-wave decomposition. The so-called semi-local momentum-space (SMS) regularization developed by the Bochum group has however shown some advantages over the non-local regularization for the case of NN and 3NF forces [48]. The application of the SMS regularization to chiral YNN forces will be studied in [49]. Finally, Fig. 3 displays the 2π -, 1π -exchange and contact ΛNN matrix elements, $\langle p'_{12}q'_3\alpha'_{\text{ANN}} = 1 | V^{\Lambda\text{NN}} | p_{12}q_3\alpha_{\text{ANN}} = 1 \rangle$, in several par-

tial-wave states $(J^\pi, T) = (1/2^+, 0), (1/2^+, 1), (3/2^+, 0)$ and $(3/2^+, 1)$ as a function of the hyperspherical coordinate $\xi^2 = p_{12}^2 + \frac{3}{4}q_3^2$ and at a hyperangle $\tan\theta = p_{12}/(\sqrt{3}/2q_3) = \frac{\pi}{4}$. Also here the non-local regularization function with a cutoff of $\Lambda = 550 \text{ MeV}$ has been applied to all potentials. The $V^{\Lambda\text{NN}}$ matrix elements in the $(3/2^+, 1)$ state have been scaled by a factor of 10 in order to make them visible on the plot. In general, the matrix elements in the higher partial-wave states that are not shown in Fig. 3 are of at least two order of magnitude smaller than the ones in the $(1/2^+, 0)$ state.

4 $A = 3 - 5$ hypernuclei with chiral ΛNN

In this section, we will investigate the possible contributions of the chiral ΛNN potentials to the separation

J=1/2 ⁺ , T=0		V _{1π}			V _{ct}		
α' _{ANN}	α _{ANN}	aPWD	IPWD	diff [%]	aPWD	IPWD	diff [%]
1	1	0.166474E-02	0.167123E-02	0.4	0.379766E-02	0.380185E-02	0.1
2	1	0.156132E-02	0.156852E-02	0.4	0.0	0.0	
3	1	-0.271857E-12	0.0		0.0	0.0	
1	2	0.156197E-02	0.156852E-02	0.4	0.0	0.0	
2	2	0.479602E-02	0.481549E-02	0.4	-0.249311E-08	-0.906432E-10	
3	2	0.476842E-13	0.0		-0.181852E-13	0.0	
1	3	0.317498E-13	0.0		0.0	0.0	
2	3	0.857880E-13	0.0		0.0	0.0	
3	3	0.503546E-04	0.505587E-04	0.4	-0.0	0.603799E-19	

Table 3: Contact and 1π -exchange ΛNN matrix elements in fm^5 , computed with the automatic partial-wave decomposition (aPWD) and the approach that exploits the locality of the chiral YNN interaction (IPWD). The incoming and outgoing momenta are fixed to $p'_{12} = p_{12} = q_3 = 0.205507 \text{ fm}^{-1}$ and $q'_3 = 0.306967 \text{ fm}^{-1}$. LECs are set to $D'_1 = 0$, $D'_2 = \frac{2C}{9f_0^2\Delta} = 0.6268 \text{ fm}^3$ with $C = 3/4 g_A$ and $f_0 = 93 \text{ MeV}$, $\Delta = 300 \text{ MeV}$, and $C'_2 = 0$, $C'_1 = C'_3 = \frac{1}{72f_0^4\Delta} = 0.1852 \text{ fm}^5$.

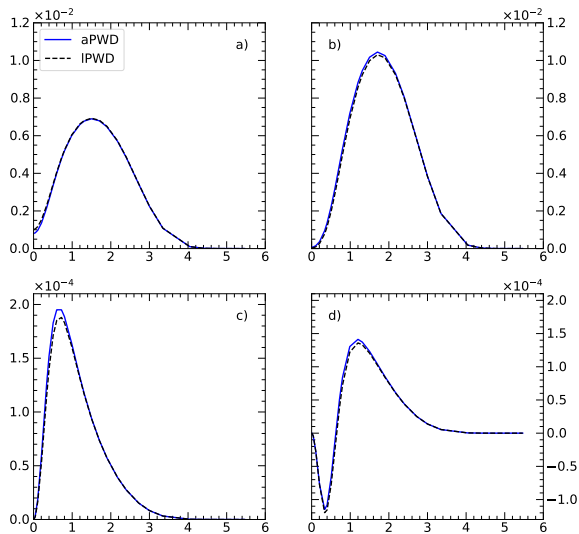


Fig. 2: 2π (right panels) and 1π (left panels) ΛNN matrix elements $\langle p'_{12} = 0.20550664, q'_3 = 0.20550664, \alpha'_{\Lambda\text{NN}} | V^{\Lambda\text{NN}} | p_{12}, q_3 = 0.20550664, \alpha_{\Lambda\text{NN}} \rangle$, computed using aPWD (solid lines) and IPWD (dashed line), as a function of p_{12} in the $(J^\pi, T) = (1/2^+, 0)$ partial-wave state and for $(\alpha'_{\Lambda\text{NN}}, \alpha_{\Lambda\text{NN}})$: a), b) (1,1), c), d) (2,2). All matrix elements are in fm^5 and have been regularized with a cutoff of $\Lambda = 550 \text{ MeV}$

energies of $A = 3 - 5$ hypernuclei. As one can see from Eqs. (4-6), the ΛNN potential is characterized by five LECs ($C'_1 - C'_3$, D'_1 , D'_2) which are difficult to determine due to the scarcity of the experimental data. However, using the decuplet saturation approximation the LECs can be qualitatively estimated. Specifically, they can be expressed in terms of contact interactions for $BB \rightarrow BB^*$, with pertinent LECs denoted by H_i in Ref. [50]. Then we are left with only one unknown LEC ($H' = H_1 + 3H_2$) for the case of $V_{\Lambda\text{NN}}$ (and two LECs when both ΛNN and ΣNN are considered) [50],

$$\begin{aligned}
C'_1 = C'_3 &= \frac{H'^2}{72\Delta}, & C'_2 &= 0, \\
D'_1 &= 0, & D'_2 &= \frac{2CH'}{9\Delta}, \\
3b_0 + b_D &= 0, & 2b_2 + 3b_4 &= -\frac{C^2}{\Delta}.
\end{aligned} \tag{12}$$

Here Δ is the decuplet-octet baryon mass difference and $C = 3/4 g_A \approx 1$ is the $B^*B\phi$ coupling constant [50]. As evidenced by Eq. (12), decuplet saturation fixes also the sub-leading meson-baryon LECs, i.e. the b_i . Note, however, that within decuplet saturation some LECs are zero and thus the most general structure of the YNN forces is not explored.

In general, the remaining LEC is expected to be determined via a fit to the binding energies of the s-shell hypernuclei, which is beyond the scope of this study and will be thoroughly studied in a separate application [49]. For our purpose of exploring the chiral ΛNN interactions here, it is sufficient to assume a realistic

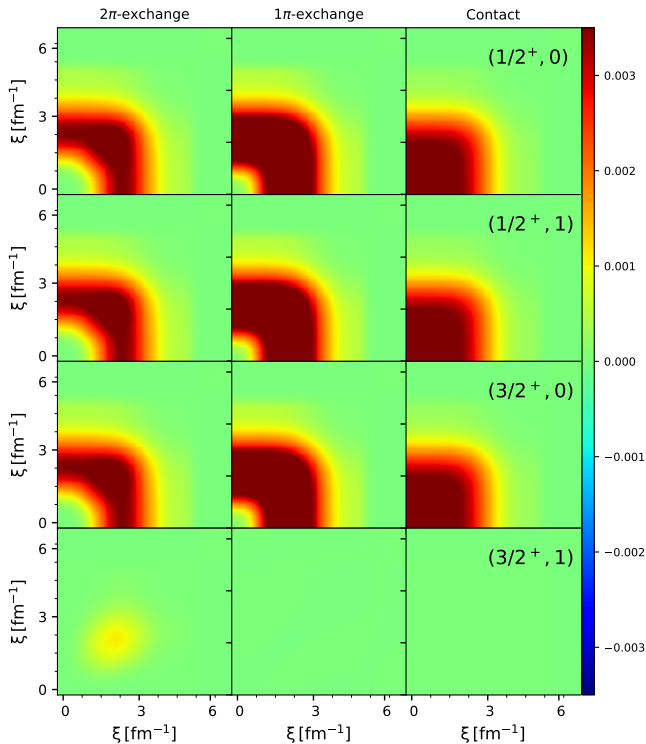


Fig. 3: Matrix elements of 2π -, 1π - and contact-ANN potentials $\langle p'_{12}q'_3\alpha'_{\text{ANN}} | V_{\text{ANN}} | p_{12}q_3\alpha_{\text{ANN}} \rangle$ as a function of the hypermomentum $\xi^2 = p_{12}^2 + \frac{3}{4}q_3^2$ at a hyperangle $\tan\theta = p_{12}/(\sqrt{3}/2q_3) = \frac{\pi}{4}$ and in different partial-wave states with $(J^\pi, T) = (1/2^+, 0), (1/2^+, 1), (3/2^+, 0), (3/2^+, 1)$. All matrix elements are in fm^5 and have been regularized with a cutoff of $\Lambda = 550$ MeV. The matrix elements in the partial wave state $(J^\pi, T) = (3/2^+, 1)$ have been multiplied by a factor of 10 in order to make them more visible.

scale for H' . Therefore, we will adopt $H' = 1/f_0^2$, as suggested in [50] based on dimensional scaling arguments, for all the calculations presented in this section. The separation energies for $A = 3-5$ hypernuclei, computed using the two-body YN potential NLO19 with a cutoff of $\Lambda = 550$ MeV in combination with the 2π -, 1π -exchange and contact ANN potentials, are listed in Table 4. The semi-local momentum-space (SMS) NN and 3N forces at N^4LO^+ and N^2LO , likewise regularized with a cutoff of $\Lambda = 550$ MeV, have been employed for describing the nuclear interaction. For $A = 4, 5$ hypernuclei also 3NFs contribute, for which we take the leading SMS regularized chiral 3NFs as specified for example in Table 1 of Ref. [40]. For the calculations with the NCSM, all interactions have been evolved with the similarity renormalization group (SRG) at a flow pa-

rameter of $\lambda = 1.88 \text{ fm}^{-1}$ up to induced 3BFs (in 3N , ΛNN and ΣNN). We have carefully checked that, for this flow parameter and using interactions up to the three-body level, the uncertainty due to omitted induced many-body forces is negligible (see also [40]). At the same time, NCSM calculations converge in reasonably sized model spaces [4, 39, 40]. As discussed in the previous section, the chiral ANN potential matrix elements at partial-wave states with the total angular momentum $J \geq 5/2$ are very small, their contributions to the binding energies are therefore expected to be insignificant. Indeed, we have observed that the ANN 3BFs with $J = 5/2$ contribute only a few keV to the binding energies in the $A = 4, 5$ systems. Therefore, for the calculations for $A \geq 4$ systems, the ANN matrix elements V^{ANN} with $J \geq 7/2$ will be omitted, whereas all the possible isospin states $T = 0, 1, 2$ and parities are taken into account.

As already mentioned, for the ${}^3_\Lambda\text{H}$ system, we provide results from both the NCSM [39, 40] and the Faddeev approach [24]. The energies for the $A = 4, 5$ systems have been computed only within the NCSM. Clearly, the difference between the two $A = 3$ results are smaller than the estimated uncertainty for the NCSM approach. The contribution of the contact potential V_{ct}^{ANN} to $B_\Lambda({}^3_\Lambda\text{H})$ is negligibly small and repulsive, whereas the $V_{2\pi}^{\text{ANN}}$ and $V_{1\pi}^{\text{ANN}}$ contributions are sizable and attractive, amounting to about 70 and 40 keV, respectively. Similarly, the effect of V_{ct}^{ANN} to the binding energy $B_\Lambda({}^4_\Lambda\text{He}, 0^+)$ is repulsive but with 30 keV rather insignificant. It becomes, however, moderately repulsive in the ${}^4_\Lambda\text{He}(1^+)$ and ${}^5_\Lambda\text{He}$ states, contributing about 50 and 200 keV, respectively. Interestingly, both the 1^+ state in the $A = 4$ system and ${}^5_\Lambda\text{He}$ are largely overbound with the 2π - and 1π -exchange ANN potentials, with respect to the present experimental information [51], while the ground state in $A = 4$ remains underbound. Since the sign of the LECs parameterizing the contact interaction is largely determined within the decuplet approximation, it could be expected that the contribution from the contact terms remains repulsive for any combinations of the H_1 and H_2 LECs. Note however that different choices for H' allow for a partial cancelation of $V_{2\pi}^{\text{ANN}}$ and $V_{1\pi}^{\text{ANN}}$. In addition, let us also mention that the inclusion of the chiral ΣNN potentials does not change the behaviour observed in these light hypernuclei. A careful analysis of the H' or H_1 and H_2 dependence of the separation energies of the s -shell hypernuclei is beyond the scope of this work.

		w/o ANN	w. 2π -ex ANN	w. 1π -ex ANN	w. ct ANN	Exp. [51]
NCSM	${}^3_{\Lambda}\text{H}$	0.080 ± 0.006	0.153 ± 0.004	0.121 ± 0.005	0.076 ± 0.007	0.164 ± 0.043
FY		0.087	0.152	0.129	0.080	
NCSM	${}^4_{\Lambda}\text{He}(0^+)$	1.432 ± 0.010	1.810 ± 0.006	1.619 ± 0.007	1.400 ± 0.010	2.347 ± 0.036
	${}^4_{\Lambda}\text{He}(1^+)$	1.164 ± 0.014	1.744 ± 0.007	1.427 ± 0.009	1.117 ± 0.016	0.942 ± 0.036
	${}^5_{\Lambda}\text{He}$	3.174 ± 0.020	4.618 ± 0.011	3.757 ± 0.034	2.961 ± 0.031	3.102 ± 0.030

Table 4: Separation energies for s-shell Λ hypernuclei without ANN 3BF and with 2π -exchange, 1π -exchange, or contact 3BF. All calculations are based on the SMS $\text{N}^4\text{LO}^+(550)$ and $\text{NLO19}(550)$ potentials for NN and YN, respectively, and on chiral ANN 3BFs with non-local regulator of $\Lambda = 550$ MeV. For the NCSM calculations all potentials have been SRG-evolved at a flow parameter of $\lambda = 1.88 \text{ fm}^{-1}$. Also, an uncertainty estimate for the results is provided.

5 Conclusions

In this work, we examined two different approaches, IPWD and aPWD, to efficiently perform the partial-wave decomposition of three-body forces, for the chiral ANN (YNN) interactions. The ANN matrix elements of the two methods were compared with each other in detail. In general, an agreement of better than 0.1% is observed for the 2π -exchange potential, whereas the difference in all the 1π -exchange and contact ANN potentials matrix elements is smaller than 0.5%. Such a benchmark provides a solid confirmation of the correctness of our implementations and is of importance for any future calculations that include the chiral YNN 3BFs.

As first application, we explored the possible impact of the leading chiral ANN potential on the separation energies of light hypernuclei. The sub-leading meson-baryon LECs appearing in the 2π -exchange 3BF and the LECs in the 1π -exchange contribution and the six-baryon contact term were estimated via decuplet saturation and assuming values for the LECs based on dimensional scaling arguments. It turned out that the weakly repulsive ANN contact interaction leads to a small contribution to the binding energies in all $A = 3 - 5$ hypernuclei, whereas the two other contributions, $V_{2\pi}^{\text{ANN}}$ and $V_{1\pi}^{\text{ANN}}$, are moderately attractive for our choice of the only remaining, LEC H' . The size of the individual contributions are significant even for ${}^3_{\Lambda}\text{H}$. This is somewhat surprising since estimates for chiral N^2LO contributions so far indicated negligible ANN force contributions [38, 40]. But the case studied here also leads to overbinding for the $J^\pi = 1^+$ state of ${}^4_{\Lambda}\text{He}$ and ${}^5_{\Lambda}\text{He}$ while ${}^4_{\Lambda}\text{He}(0^+)$ is still clearly underbound. The interesting question whether one can determine an optimal

combination of the LECs within the decuplet approximation so that all light hypernuclei are well described, should be and will be addressed in a future study. In such a study, it should also be addressed whether the ANN force contribution to ${}^3_{\Lambda}\text{H}$ remains sizable.

Acknowledgements HL, JH, UGM and AN thank Stefan Petschauer for collaboration at the early stage of this work. This project is part of the ERC Advanced Grant “EXOTIC” supported the European Research Council (ERC) under the European Union’s Horizon 2020 research and innovation programme (grant agreement No. 101018170). This work is further supported in part by the Deutsche Forschungsgemeinschaft (DFG, German Research Foundation) and the NSFC through the funds provided to the Sino-German Collaborative Research Center TRR110 “Symmetries and the Emergence of Structure in QCD” (DFG Project ID 196253076 - TRR 110, NSFC Grant No. 12070131001), and by the MKW NRW under the funding code NW21-024-A. The work of HK, MK and KM is supported by Japan Society for the Promotion of Science (JSPS) KAKENHI Grants No. JP19K03849 and No. JP22K03597. The work of UGM was supported in part by The Chinese Academy of Sciences (CAS) President’s International Fellowship Initiative (PIFI) (grant no. 2025PD0022). We also acknowledge support of the THEIA net-working activity of the Strong 2020 Project. The numerical calculations were performed on JURECA of the Jülich Supercomputing Centre, Jülich, Germany.

References

1. A. Nogga, H. Kamada, W. Glöckle, and B. R. Barrett. The α -particle based on modern nuclear forces. *Phys. Rev. C*, 65(5):054003, 2002.
2. E. Epelbaum et al. Few- and many-nucleon systems with semilocal coordinate-space regularized chiral two- and three-body forces. *Phys. Rev. C*, 99(2):024313, 2019. [arXiv:1807.02848](https://arxiv.org/abs/1807.02848), [doi:10.1103/PhysRevC.99.024313](https://doi.org/10.1103/PhysRevC.99.024313).
3. S. Binder et al. Few-nucleon systems with state-of-the-art chiral nucleon-nucleon forces. *Phys. Rev. C*,

- 93(4):044002, 2016. [arXiv:1505.07218](#), [doi:10.1103/PhysRevC.93.044002](#).
4. P. Maris et al. Nuclear properties with semilocal momentum-space regularized chiral interactions beyond N^2 LO. *Phys. Rev. C*, 106(6):064002, 2022. [arXiv:2206.13303](#), [doi:10.1103/PhysRevC.106.064002](#).
 5. N. Kalantar-Nayestanaki, E. Epelbaum, J. G. Messchendorp, and A. Nogga. Signatures of three-nucleon interactions in few-nucleon systems. *Rept. Prog. Phys.*, 75:016301, 2012. [arXiv:1108.1227](#), [doi:10.1088/0034-4885/75/1/016301](#).
 6. L. Girlanda, E. Filandri, A. Kievsky, L. E. Marcucci, and M. Viviani. Effect of the N^3 LO three-nucleon contact interaction on p-d scattering observables. *Phys. Rev. C*, 107(6):L061001, 2023. [arXiv:2302.03468](#), [doi:10.1103/PhysRevC.107.L061001](#).
 7. R. Lazauskas, J. Carbonell, A. C. Fonseca, M. Viviani, A. Kievsky, and S. Rosati. Low energy n- 3 H scattering: A Novel testground for nuclear interaction. *Phys. Rev. C*, 71:034004, 2005. [arXiv:nucl-th/0412089](#), [doi:10.1103/PhysRevC.71.034004](#).
 8. A. Deltuva and A. C. Fonseca. Four-body calculation of $^2\text{H}(d,p)^3\text{H}$ and $^2\text{H}(d,n)^3\text{He}$ reactions above breakup threshold. *Phys. Rev. C*, 95(2):024003, 2017. [arXiv:1702.01034](#), [doi:10.1103/PhysRevC.95.024003](#).
 9. M. Piarulli et al. Light-nuclei spectra from chiral dynamics. *Phys. Rev. Lett.*, 120(5):052503, 2018. [arXiv:1707.02883](#).
 10. Takaharu Otsuka, Toshio Suzuki, Jason D. Holt, Achim Schwenk, and Yoshinori Akaishi. Three-body forces and the limit of oxygen isotopes. *Phys. Rev. Lett.*, 105:032501, 2010. [arXiv:0908.2607](#), [doi:10.1103/PhysRevLett.105.032501](#).
 11. T. Cornelius, W. Glöckle, J. Haidenbauer, Y. Koike, W. Plessas, and H. Witala. Predictions of the Paris N-N potential for three-nucleon continuum observables: Comparison of two approaches. *Phys. Rev. C*, 41:2538–2543, 1990. [doi:10.1103/PhysRevC.41.2538](#).
 12. James Lewis Friar et al. Benchmark solutions for a model three-nucleon scattering problem. *Phys. Rev. C*, 42:1838–1840, 1990. [doi:10.1103/PhysRevC.42.1838](#).
 13. J. L. Friar, G. L. Payne, W. Glöckle, D. Huber, and H. Witala. Benchmark solutions for n-d breakup amplitudes. *Phys. Rev. C*, 51:2356–2359, 1995. [doi:10.1103/PhysRevC.51.2356](#).
 14. A. Nogga, A. Kievsky, H. Kamada, Walter Glöckle, L.E. Marcucci, S. Rosati, and M. Viviani. The Three nucleon bound state using realistic potential models. *Phys. Rev. C*, 67:034004, 2003. [arXiv:nucl-th/0202037](#), [doi:10.1103/PhysRevC.67.034004](#).
 15. H. Kamada et al. Benchmark test calculation of a four nucleon bound state. *Phys. Rev. C*, 64:044001, 2001. [arXiv:nucl-th/0104057](#), [doi:10.1103/PhysRevC.64.044001](#).
 16. M. Viviani, A. Deltuva, R. Lazauskas, J. Carbonell, A. C. Fonseca, A. Kievsky, L. E. Marcucci, and S. Rosati. Benchmark calculation of n- 3 H and p- 3 He scattering. *Phys. Rev. C*, 84:054010, 2011. [arXiv:1109.3625](#), [doi:10.1103/PhysRevC.84.054010](#).
 17. M. Viviani, A. Deltuva, R. Lazauskas, A. C. Fonseca, A. Kievsky, and L. E. Marcucci. Benchmark calculation of p- 3 H and n- 3 He scattering. *Phys. Rev. C*, 95(3):034003, 2017. [arXiv:1610.09140](#), [doi:10.1103/PhysRevC.95.034003](#).
 18. K. Miyagawa and W. Glöckle. Hypertriton calculation with meson theoretical nucleon-nucleon and hyperon nucleon interactions. *Phys. Rev. C*, 48:2576, 1993. [doi:10.1103/PhysRevC.48.2576](#).
 19. K. Miyagawa, H. Kamada, W. Glöckle, and V.G.J. Stoks. Properties of the bound $\Lambda(\Sigma)NN$ system and hyperon nucleon interactions. *Phys. Rev. C*, 51:2905, 1995. [doi:10.1103/PhysRevC.51.2905](#).
 20. E. Hiyama, M. Kamimura, T. Motoba, T. Yamada, and Y. Yamamoto. $\Lambda - \Sigma$ conversion in $^4_\Lambda\text{He}$ and $^4_\Lambda\text{H}$ based on a four-body calculation. *Phys. Rev. C*, 65:011301, 12 2001. URL: <https://link.aps.org/doi/10.1103/PhysRevC.65.011301>.
 21. A. Nogga, H. Kamada, and W. Glöckle. The Hypernuclei $^4_\Lambda\text{He}$ and $^4_\Lambda\text{H}$: Challenges for modern hyperon nucleon forces. *Phys. Rev. Lett.*, 88:172501, 2002. [arXiv:nucl-th/0112060](#), [doi:10.1103/PhysRevLett.88.172501](#).
 22. H. Nemura, Y. Akaishi, and Y. Suzuki. Ab initio approach to s shell hypernuclei hypertriton, hyperHe-4(Lambda), hyperHe-4(Lambda) and hyperHe-5(Lambda) with a realistic Lambda N - Sigma N interaction. *Phys. Rev. Lett.*, 89:142504, 2002. [arXiv:nucl-th/0203013](#), [doi:10.1103/PhysRevLett.89.142504](#).
 23. S. Petschauer, N. Kaiser, J. Haidenbauer, U.-G. Meißner, and W. Weise. Leading three-baryon forces from SU(3) chiral effective field theory. *Phys. Rev. C*, 93(1):3, January 2016. URL: <http://link.aps.org/doi/10.1103/PhysRevC.93.014001>, [doi:10.1103/PhysRevC.93.014001](#).
 24. H. Kamada, M. Kohno, and K. Miyagawa. Faddeev calculation of $^3_\Lambda\text{H}$ incorporating the 2π -exchange ΛNN interaction. *Phys. Rev. C*, 108(2):024004, 2023. [arXiv:2304.06352](#), [doi:10.1103/PhysRevC.108.024004](#).
 25. M. Kohno, H. Kamada, and K. Miyagawa. Contributions of 2π exchange, 1π exchange, and contact three-body forces in NNLO chiral effective field theory to $^3_\Lambda\text{H}$. *Phys. Rev. C*, 109(2):024003, 2024. [arXiv:2311.10923](#), [doi:10.1103/PhysRevC.109.024003](#).
 26. I. R. Afnan and B. F. Gibson. ΛN - ΣN coupling in $^3_\Lambda\text{H}$. *Phys. Rev. C*, 40:R7–R9, 1989. [doi:10.1103/PhysRevC.40.R7](#).
 27. Y. Fujiwara, Y. Suzuki, M. Kohno, and K. Miyagawa. Addendum: Triton and hypertriton binding energies calculated from SU(6) quark-model baryon-baryon interactions. *Phys. Rev. C*, 77:027001, 2008. [arXiv:0710.0047](#), [doi:10.1103/PhysRevC.77.027001](#).
 28. H. Garcilazo, T. Fernandez-Carames, and A. Valcarce. ΛNN and ΣNN systems at threshold. *Phys. Rev. C*, 75:034002, 2007. [arXiv:hep-ph/0701275](#), [doi:10.1103/PhysRevC.75.034002](#).
 29. R. Wirth, D. Gazda, P. Navrátil, A. Calci, J. Langhammer, and R. Roth. Ab Initio Description of p-Shell Hypernuclei. *Phys. Rev. Lett.*, 113(19):192502, 2014. [arXiv:1403.3067](#), [doi:10.1103/PhysRevLett.113.192502](#).
 30. R. Wirth, D. Gazda, P. Navrátil, and R. Roth. Hypernuclear No-Core Shell Model. *Phys. Rev. C*, 97(6):064315, 2018. [arXiv:1712.05694](#), [doi:10.1103/PhysRevC.97.064315](#).
 31. L. Contessi, N. Barnea, and A. Gal. Resolving the Λ Hypernuclear Overbinding Problem in Pionless Effective Field Theory. *Phys. Rev. Lett.*, 121(10):102502, 2018. [arXiv:1805.04302](#), [doi:10.1103/PhysRevLett.121.102502](#).
 32. Dillon Frame, Timo A. Lähde, Dean Lee, and Ulf-G. Meißner. Impurity Lattice Monte Carlo for Hypernuclei. *Eur. Phys. J. A*, 56(10):248, 2020. [arXiv:2007.06335](#), [doi:10.1140/epja/s10050-020-00257-y](#).
 33. H. Le, J. Haidenbauer, U.-G. Meißner, and A. Nogga. Jacobi no-core shell model for p-shell hypernuclei. *Eur. Phys. J. A*, 56(12):301, 2020. [arXiv:2008.11565](#), [doi:10.1140/epja/s10050-020-00314-6](#).
 34. Fabian Hildenbrand, Serdar Elhatisari, Zhengxue Ren, and Ulf-G. Meißner. Towards Hypernuclei from Nuclear Lattice Effective Field Theory. 6 2024. [arXiv:2406.17638](#).

35. F. Ferrari Ruffino, N. Barnea, S. Deflorian, W. Leidemann, D. Lonardoni, G. Orlandini, and F. Pederiva. Benchmark Results for Few-Body Hypernuclei. *Few Body Syst.*, 58(3):113, 2017. [arXiv:1701.06399](#), [doi:10.1007/s00601-017-1273-7](#).
36. P. Reinert, H. Krebs, and E. Epelbaum. Semilocal momentum-space regularized chiral two-nucleon potentials up to fifth order. *Eur. Phys. J.*, A54(5):86, 2018. [arXiv:1711.08821](#), [doi:10.1140/epja/i2018-12516-4](#).
37. J. Haidenbauer, S. Petschauer, N. Kaiser, U.-G. Meißner, A. Nogga, and W. Weise. Hyperon-nucleon interaction at next-to-leading order in chiral effective field theory. *Nucl. Phys. A*, 915:24–58, 2013. [arXiv:1304.5339](#), [doi:10.1016/j.nuclphysa.2013.06.008](#).
38. J. Haidenbauer, U.-G. Meißner, and A. Nogga. Hyperon-nucleon interaction within chiral effective field theory revisited. *Eur. Phys. J. A*, 56(3):91, 2020. [arXiv:1906.11681](#), [doi:10.1140/epja/s10050-020-00100-4](#).
39. H. Le, J. Haidenbauer, U.-G. Meißner, and A. Nogga. Ab initio calculation of charge-symmetry breaking in $A=7$ and 8Λ hypernuclei. *Phys. Rev. C*, 107(2):024002, 2023. [arXiv:2210.03387](#), [doi:10.1103/PhysRevC.107.024002](#).
40. Hoai Le, Johann Haidenbauer, Ulf-G. Meißner, and Andreas Nogga. Separation energies of light Λ hypernuclei and their theoretical uncertainties. *Eur. Phys. J. A*, 60(1):3, 2024. [arXiv:2308.01756](#), [doi:10.1140/epja/s10050-023-01219-w](#).
41. H. Kamada, M. Kohno, and K. Miyagawa. Erratum, in preparation.
42. Stefan Petschauer. *Baryonic forces and hyperons in nuclear matter from $SU(3)$ chiral effective field theory*. PhD thesis, Technische Universität München, 2016. URL: <https://mediatum.ub.tum.de/1285353>.
43. Maxim Mai, Peter C. Bruns, Bastian Kubis, and Ulf-G. Meißner. Aspects of meson-baryon scattering in three and two-flavor chiral perturbation theory. *Phys. Rev. D*, 80:094006, 2009. [arXiv:0905.2810](#), [doi:10.1103/PhysRevD.80.094006](#).
44. M. Kohno, H. Kamada, and K. Miyagawa. Partial-wave expansion of ANN three-baryon interactions in chiral effective field theory. *Phys. Rev. C*, 106(5):054004, 2022. [arXiv:2208.02388](#), [doi:10.1103/PhysRevC.106.054004](#).
45. K. Hebel, H. Krebs, E. Epelbaum, J. Golak, and R. Skibinski. Efficient calculation of chiral three-nucleon forces up to $N^3\text{LO}$ for ab-initio studies. *Phys. Rev. C*, 91(4):044001, 2015. [arXiv:1502.02977](#), [doi:10.1103/PhysRevC.91.044001](#).
46. R. Skibinski, J. Golak, K. Topolnicki, H. Witala, H. Kamada, W. Glöckle, and A. Nogga. The Tucson-Melbourne Three-Nucleon Force in the automatized Partial Wave Decomposition. *Eur. Phys. J. A*, 47:48, 2011. [arXiv:1101.2150](#), [doi:10.1140/epja/i2011-11048-9](#).
47. W. Glöckle. *The Quantum Mechanical Few-Body Problem*. Springer-Verlag, Berlin-Heidelberg, 1983.
48. E. Epelbaum, H. Krebs, and P. Reinert. *Semi-local Nuclear Forces From Chiral EFT: State-of-the-Art and Challenges*, pages 1–25. Springer, 2022. [arXiv:2206.07072](#), [doi:10.1007/978-981-15-8818-1_54-1](#).
49. H. Le, J. Haidenbauer, U.-G. Meißner, and A. Nogga. in preparation.
50. S. Petschauer, J. Haidenbauer, N. Kaiser, U.-G. Meißner, and W. Weise. Density-dependent effective baryon-baryon interaction from chiral three-baryon forces. *Nucl. Phys. A*, 957:347–378, 2017. [arXiv:1607.04307](#), [doi:10.1016/j.nuclphysa.2016.09.010](#).
51. P. Eckert, P. Achenbach, et al. Chart of hypernucleides — Hypernuclear structure and decay data, 2021. <https://hypernuclei.kph.uni-mainz.de>.